Leadership in Sustainable Infrastructure
Leadership en Infrastructures Durables

Vancouver, Canada
May 31 – June 3, 2017/ *Mai 31 – Juin 3, 2017*

CFD STUDY OF THE AIR-ENTRAINMENT CHARACTERISTICS OF A SUBMERGED HYDRAULIC JUMP

Jesudhas, V [1], Roussinova, V [2], Balachandar, R [3], Barron, R [4] and Williams, P [5,6].
[1,2,3,4,5] University of Windsor, Canada
[6] williamq@uwindsor.ca

Abstract: Hydraulic jumps are associated with strong turbulence, free-surface fluctuations, air entrainment and energy dissipation. Over the last century, several researchers have attempted to study these characteristics experimentally. However, due to limitations of conventional measuring techniques in the air-water flow of the hydraulic jump, they were only partially successful. This paper presents the results of a three-dimensional, unsteady, detached eddy simulation of a submerged hydraulic jump with an inlet Froude number 8.2 and a submergence factor of 0.24. Volume of fluid (VOF) multiphase model is used for capturing the free-surface and the air-entrainment characteristics. The results of the simulations are validated with experimental results. The flow features of the submerged hydraulic jump captured by the simulation is presented with pertinent discussions. Since, the submergence factor of the submerged hydraulic jump is low, considerable amount of air was entrained into the flow. The mechanism of air entrainment in a submerged hydraulic jump is also analysed.

1 INTRODUCTION

When the flow transitions from a supercritical to subcritical flow in an open channel, hydraulic jumps are formed. Hydraulic jumps occurring in rectangular channels are called as classical hydraulic jumps (CHJ). They are characterized by a sharp increase in the free-surface height accompanied by strong turbulence, air entrainment and energy dissipation. The super-critical depth d_1^* and the sub-critical depth d_2^* are called sequent depths and are a function of the inlet Froude number F_1 (Chow, 1959), defined as:

$$\frac{d_2^*}{d_1^*} = 0.5\left(\sqrt{1 + 8F_1^2} - 1\right) \quad (1)$$

where F_1 is the inlet Froude number. The point where the free surface increases abruptly is called the jump toe. Starting at the jump toe, there is a region of recirculation near the free surface of CHJ called as the roller. When the tail-water depth d_2 is higher than the sub-critical sequent depth d_2^*, the toe of the hydraulic jump moves toward the sluice gate. Both the toe and the roller become submerged. This is called as the submerged hydraulic jump (SHJ). A dimensionless submergence factor $S = (d_2 - d_2^*)/d_2$ was defined by Rajaratnam (1967). A schematic of the complex flow field of SHJ is presented in Fig. 1. There is a region of forward flow near the bed resembling a wall-jet. Above the wall-jet region is the recirculation region or the roller. A shear layer is developed between the wall-jet flow region and the roller, which expands in the vertical direction as we move downstream. The distance from the sluice gate to the end of the roller is called as the length of the roller L_r, which is an important parameter in the design of stilling basins for energy dissipation in hydraulic structures. After the end of the roller region the flow transitions into a regular open channel flow.

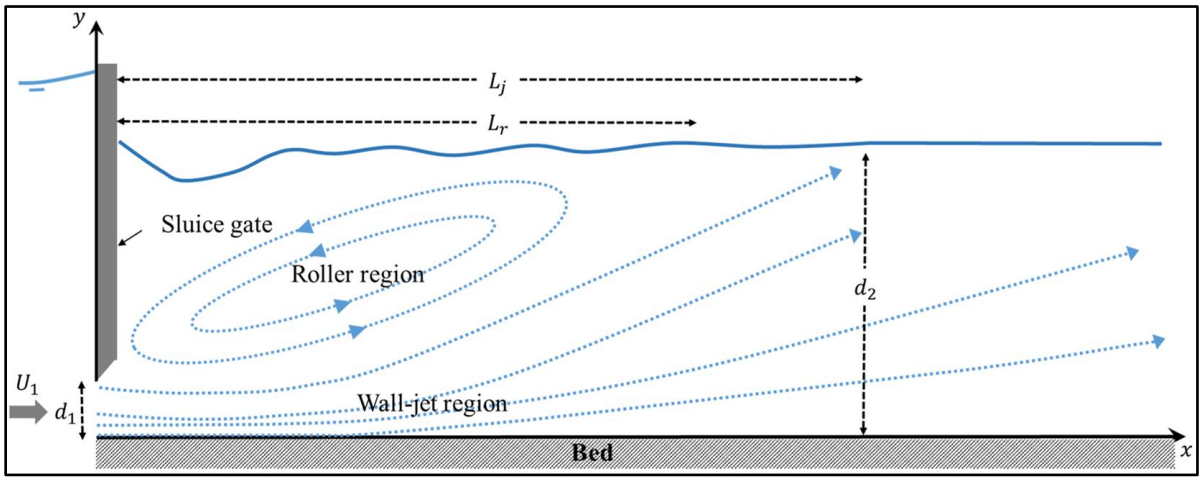

Figure 1: Schematic representation of the submerged hydraulic jump (Jesudhas et al, 2016)

To study the flow characteristics, Long et al. (1990) carried out an experimental study on SHJ using laser Doppler velocimetry (LDV). They reported the velocity field not only in the streamwise direction but also in the lateral direction. Their studies concluded that the interaction between the roller and wall-jet causes the SHJ flow field to become three-dimensional in nature. Several numerical studies were subsequently conducted on SHJ (Long et al., 1991, Ma et al., 2001 and Javan and Eghbalzadeh, 2013). However, these were two-dimensional computations and were not able to fully capture the complex three-dimensional flow field of the SHJ. To address this, a three-dimensional, unsteady, detached eddy simulation (DES) of SHJ with an inlet Froude number 8.2 and a submergence factor of 0.24 was carried out at the Department of Civil and Environmental Engineering, University of Windsor, Canada. Volume of fluid (VOF) along with high resolution interface capturing technique (HRIC) was used for capturing the free surface. A detailed analysis of the flow field along with turbulence characteristics and coherent structures was presented in Jesudhas et al. 2016.

Air entrainment in hydraulic jumps have received considerable attention by researchers. Air entrainment in SHJ not only depends on inlet Froude number F_1 but also on the submergence factor S. Since the submergence factor of the SHJ presented is low, considerable amount of air was entrained in the flow. The present paper discusses the air-entrainment characteristics of SHJ simulated in Jesudhas et al. 2016 after briefly discussing the flow features of SHJ. The mechanism of air entrainment and the instigating factor for entraining air is also analyzed.

2 THE MODEL

The DES method uses Reynolds-averaged Navier-Stokes (RANS) models close to the wall and large eddy simulation (LES) in the outer regions of the flow. Improved delayed detached eddy simulation (IDDES) available in the commercial solver STAR-CCM+ was used in the present study. The k-ω detached eddy model was selected as it is known to perform well in an adverse pressure gradient flow like the hydraulic jump. The complete formulation of this model is presented in Jesudhas (2016) and STAR-CCM+ v8.06 User Guide and hence not repeated here for brevity. The schematic of the domain used in the simulations is shown in Fig. 2. The size of the domain was selected based on the experiments of Long et al. (1990) to enable comparison with the results.

The size of the domain was 2.5 m × 0.467 m × 0.5 m. The Cartesian coordinates x, y and z are adopted as streamwise, vertical (wall-normal) and transverse directions, respectively. The origin of the coordinate system is positioned at the beginning of the inner wall of the flume. The boundary conditions used in the simulation are also presented in Fig. 2. The mesh used in the present simulation consists of about 5.6 million hexahedral cells. Refinements were made in the regions of interest and also prism layers were used near all the walls to capture the wall effects. The transient simulations were run with a time

step $\delta t = 0.001\ s$. The solution was considered to be converged when the residuals of continuity and momentum fell below 10^{-6}. The velocity statistics of the present simulation have been calculated by averaging the data for 10 s following convergence.

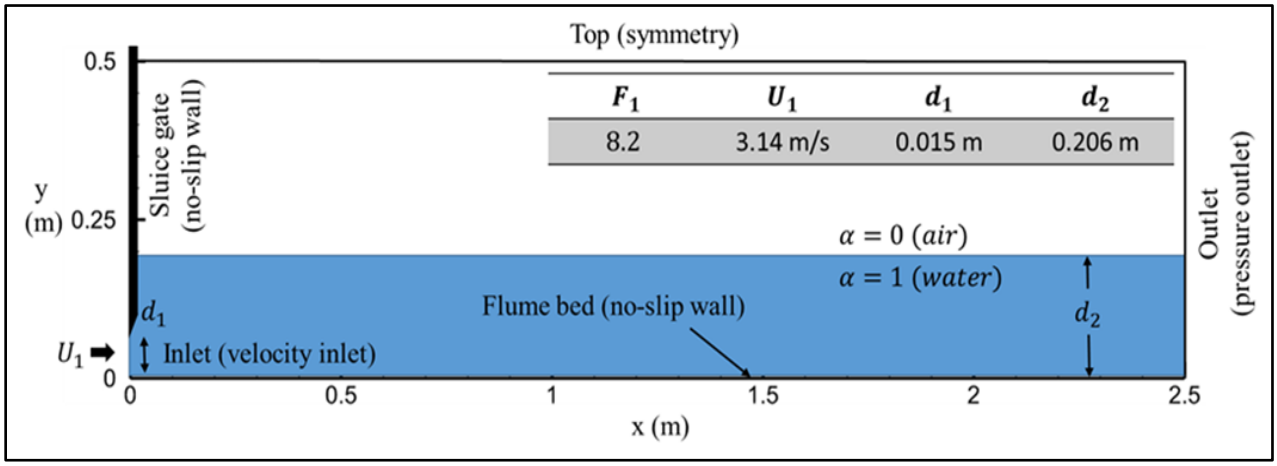

Figure 2: Schematic representation of the simulation domain at $t = 0$ s (Jesudhas et al, 2016)

3 VALIDATION

An exhaustive validation of the flow and turbulence characteristics is presented in Jesudhas et al. (2016). A sample of the validation of results is presented in Fig. 3. Fig. 3(a) shows the comparison of the mean free surface profile predicted by the present simulation to the experimental results of Long et al. (1990). The free surface decreases in height initially due to the high-speed wall jet emerging from the sluicegate, after which it increases to the tail-water depth d_2 . The location of the minimum depth in the free surface is predicted accurately by the simulations.

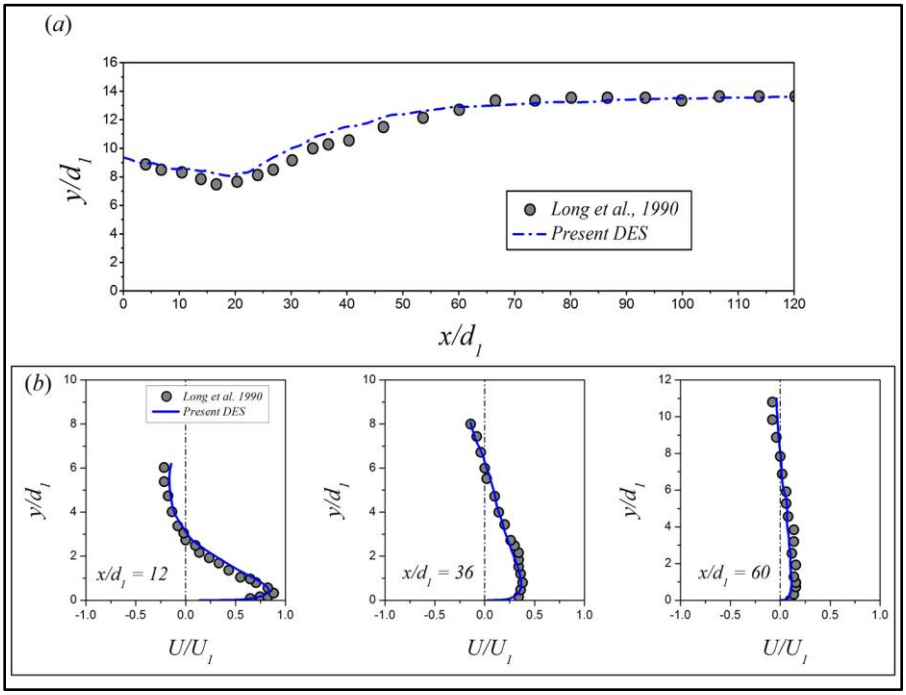

Figure 3: Validation of simulations results with the experiments of Long et al. (1990).

Immediately downstream of the minimum depth, there is a difference of 5% between the experimental and simulation results. As, mentioned earlier, considerable amount of air is entrained in the flow due to the low submergence factor of SHJ. A difference of up to 10% is considered to be satisfactory in such flow fields (Chachereau and Chanson, 2011). Fig. 3(b) presents the comparison of mean streamwise profiles between experimental and simulation results at three streamwise locations x/d_1 =12, 36 and 60. It can be seen that the simulation results agree well with the experimental results of Long et al. (1990). The mean streamwise velocity increases from zero at the bed to a positive maximum velocity U_{max} in the wall-jet region before it decreases and becomes negative in the roller region. From Fig. 3(b) it is also apparent that the value of U_{max} decreases as we move downstream i.e., from x/d_1 =12 to x/d_1 = 60. This is caused by the decay and expansion of the wall-jet flow emanating from the sluice gate. From Fig. 3 it is apparent that the results of the present simulations agree well with the experimental results of Long et al. (1990).

4 RESULTS AND DISCUSSIONS

Fig. 4 shows the three-dimensional instantaneous free surface of the SHJ. The free surface is colored using the contours of instanteous vorticity magnitude. Initially, there is a reduction in free surface height. Beyond the region of minimum depth the free surface is undulated intensely as observed in Fig. 4. This is the location were the submerged roller reaches the free surface. These undulations are caused by vortices from the shear layer impacting the free surface (Sarpkaya, 1996), which is discussed in the later part of this paper. This is evidenced by the maximum vorticity intensity in this region. Downstream of the roller, the free surface perturbations are reduced and the free surface becomes almost flat farther downstream (Fig. (4)).

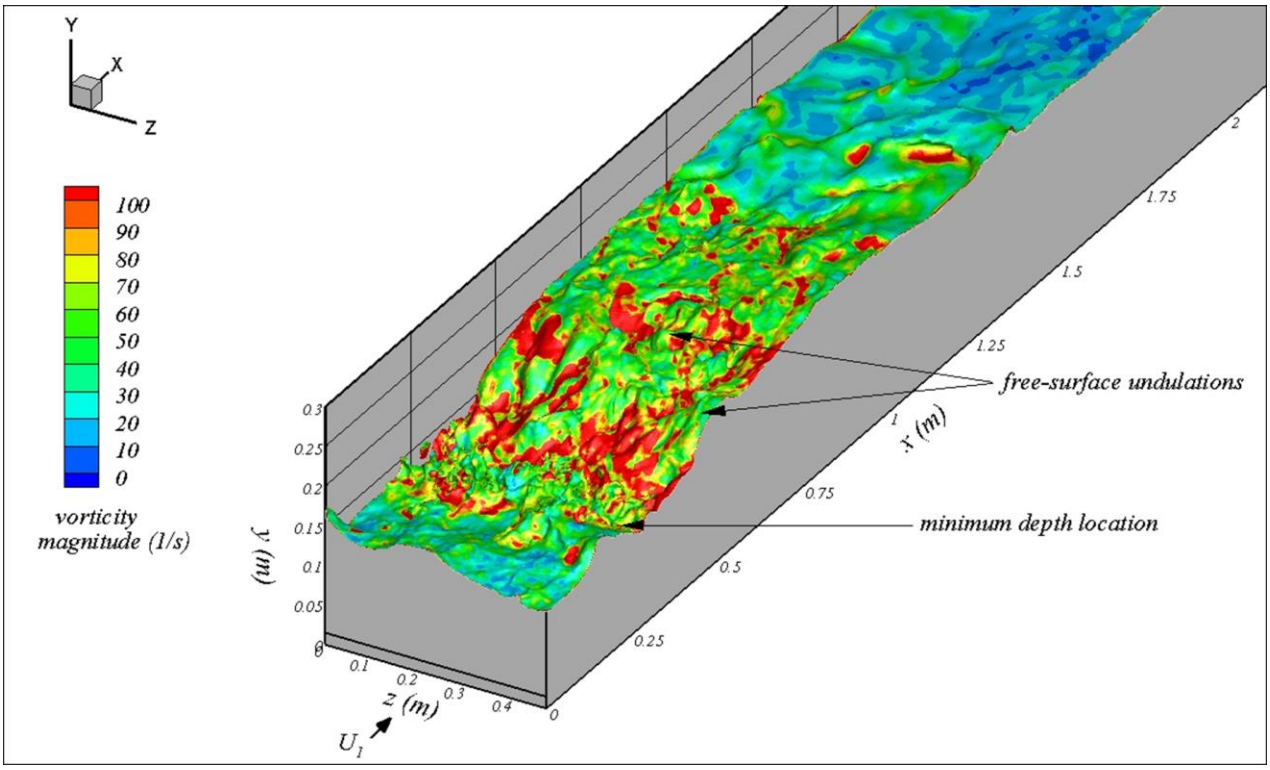

Figure 4: Three-dimensional free surface of the SHJ.

Fig.5(a) shows the contours of mean streamwise velocity in the central plane of the SHJ. The large negative region near the free-surface is part of the roller region. It extends from x/d_1 =0 to x/d_1 = 60 (Fig 5(a)). Beyond this region, the flow slowly transitions to open channel flow. However, the present simulation domain is not long enough for the flow to fully recover to a fully developed open channel flow.

The wall-jet flow emanates from the sluice gate and the region up to $x/d_1 = 10$ resembles the potential core of a wall-jet. The wall-jet decays and expands beyond $x/d_1 = 10$ as observed from Fig. 5(a). The shear layer is formed between the roller region and wall-jet region and expands in the vertical direction as we move in the streamwise direction. Fig. 5(b) shows the mean vector plots in the central plane of SHJ. The recirculation in the roller is clearly visible in Fig. 5(b). Also, plotted in Fig. 5(b) are dashed lines denoting $U = 0$ and $U = U_{max}$. The represent the upper and lower extremities of the shear layer (Jesudhas et al., 2016).

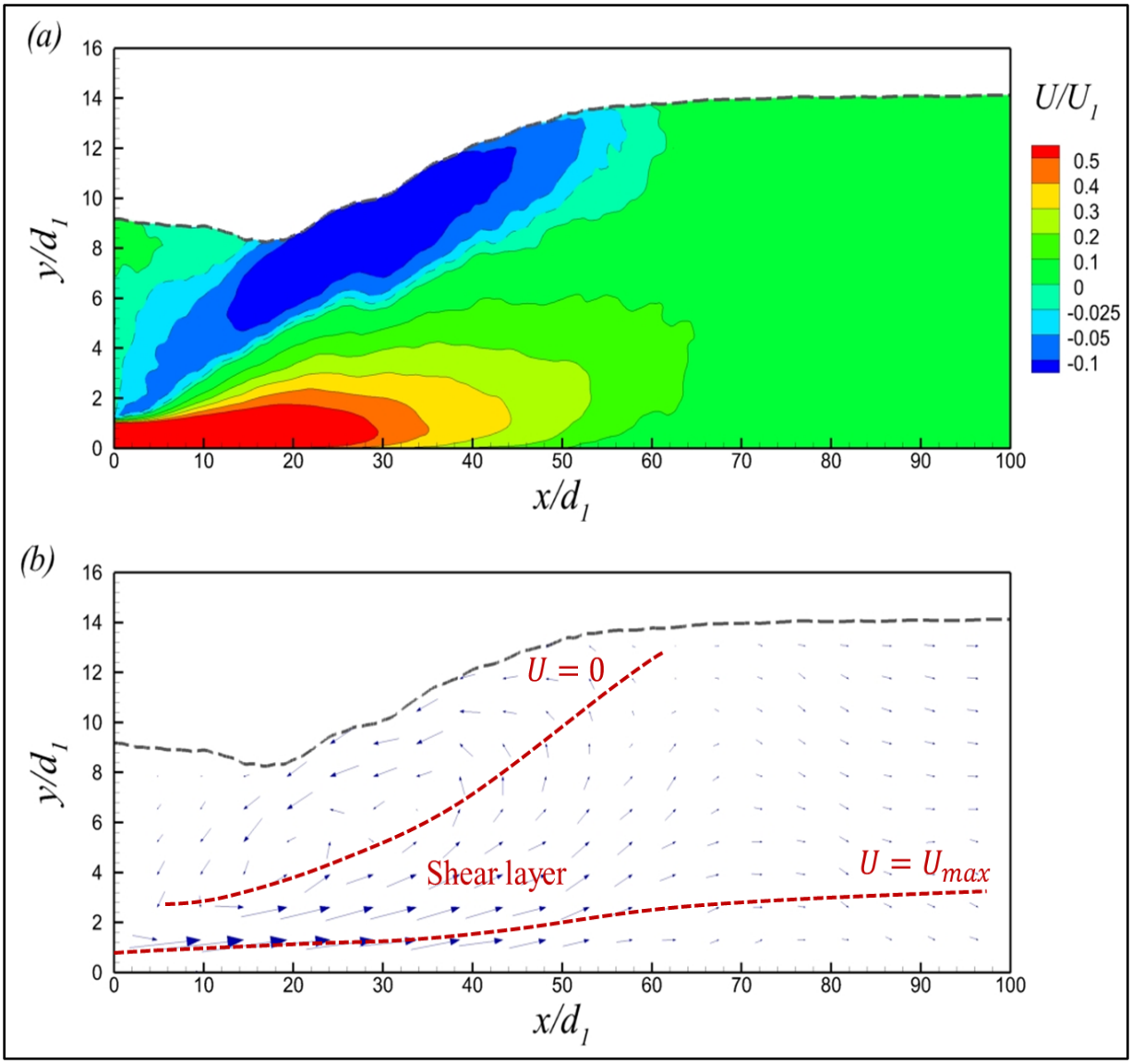

Figure 5: (a) Contours of mean streamwise velocity in the central plane of SHJ
(b) mean vector plot in the central plane of SHJ.

Fig. 6(a) shows the contours of the mean Reynolds stress in the central plane of the SHJ. It can be clearly seen that the maximum values are generated in the shear layer due to the interaction of the roller and the wall-jet. Also, the turbulence generated by the bed is not as significant as the turbulence generated in the shear layer. Figs. 6(b) and (c) shows the contours of mean stream wise and vertical fluxes of the turbulent kinetic energy given by $t_{ku} = 0.5(u^3 + uv^2 + uw^2)$ and $t_{kv} = 0.5(v^3 + u^2v + vw^2)$,

respectively. As indicated by the arrows in Figs. 6(b) and (c) it is evident the turbulent kinetic energy generated in the shear layer by the interaction of roller and wall jet is transported in the streamwise and vertical directions. This is significant because for air entrainment to occur the surface tension of the free surface must be overcome by the turbulence that is generated below the free surface (Chanson, 1995).

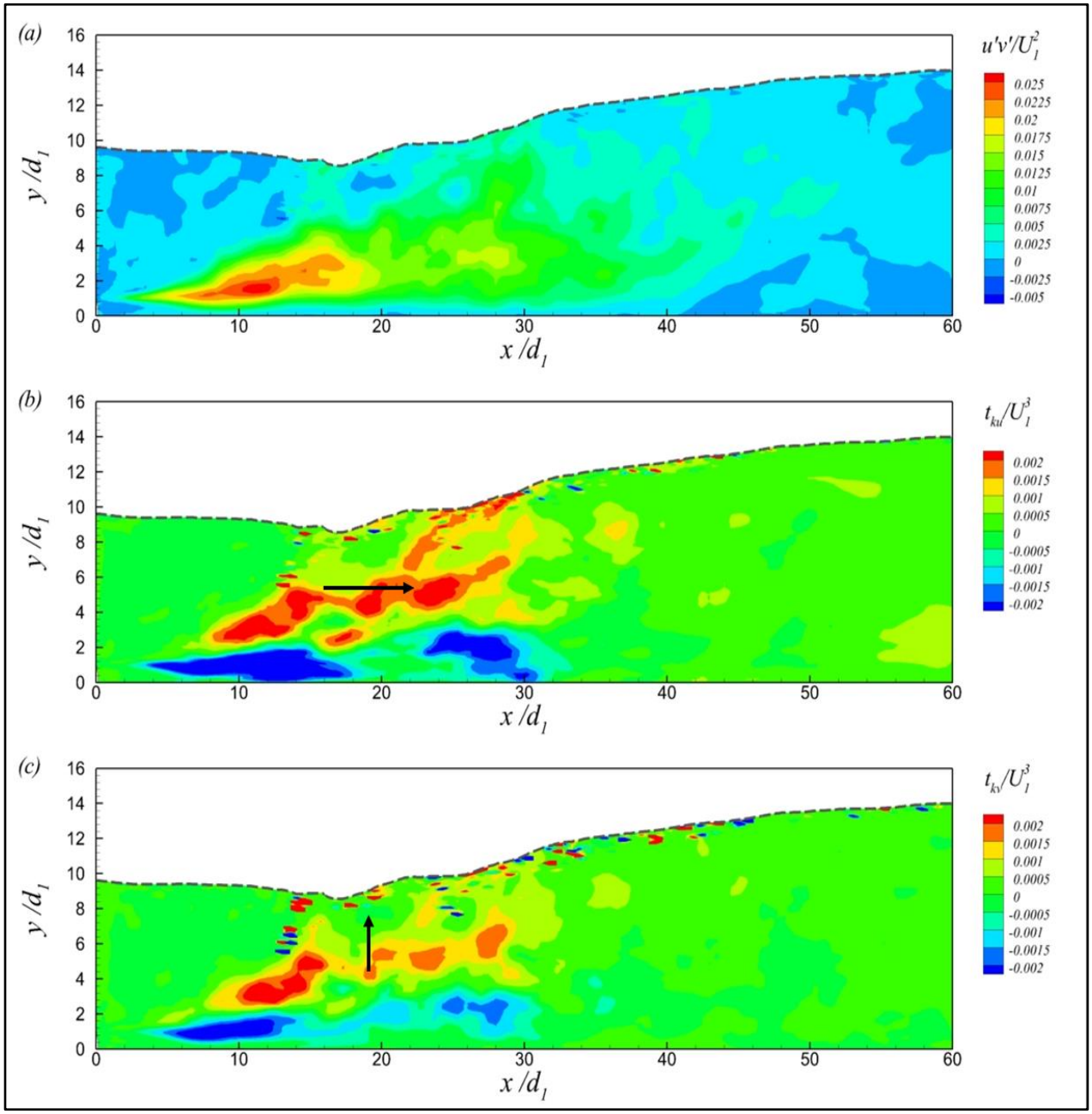

Figure 6: (a) mean Reynolds stress distribution in the central plane (b) Streamwise flux of turbulent kinetic energy (c) Vertical flux of turbulent kinetic energy.

Fig. 7(a) shows the contours of mean air concentration C in the central plane of the SHJ. It can be seen that significant amount of air is entrained into the flow. The maximum air concentration happens near the sluice gate within $x/d_1 = 15$. Beyond this there is negligible air entrainment into the flow. The variation of average air concentration C_{ave} at any streamwise location normalized by the maximum value C_{max} along the central plane is presented in Fig. 7(b). The field measurements of Valle and Pasternack (2006) for a SHJ is also plotted in Fig. 7(b) for qualitative comparison. The streamwise distance is normalized using the aeration length L_a. The peak air concentration for the SHJ occurs near the sluice gate. Also, plotted in Fig. 7(b) is a typical C_{ave} plot of a CHJ from Hager (1995). In contrast to the submerged jump, the toe of the classical hydraulic jump occurs downstream of the sluice gate consequently the maximum air concentration occurs downstream of the toe. Overall the amount of the air entrained by the CHJ is higher than the SHJ, as observed from Fig. 7(b).

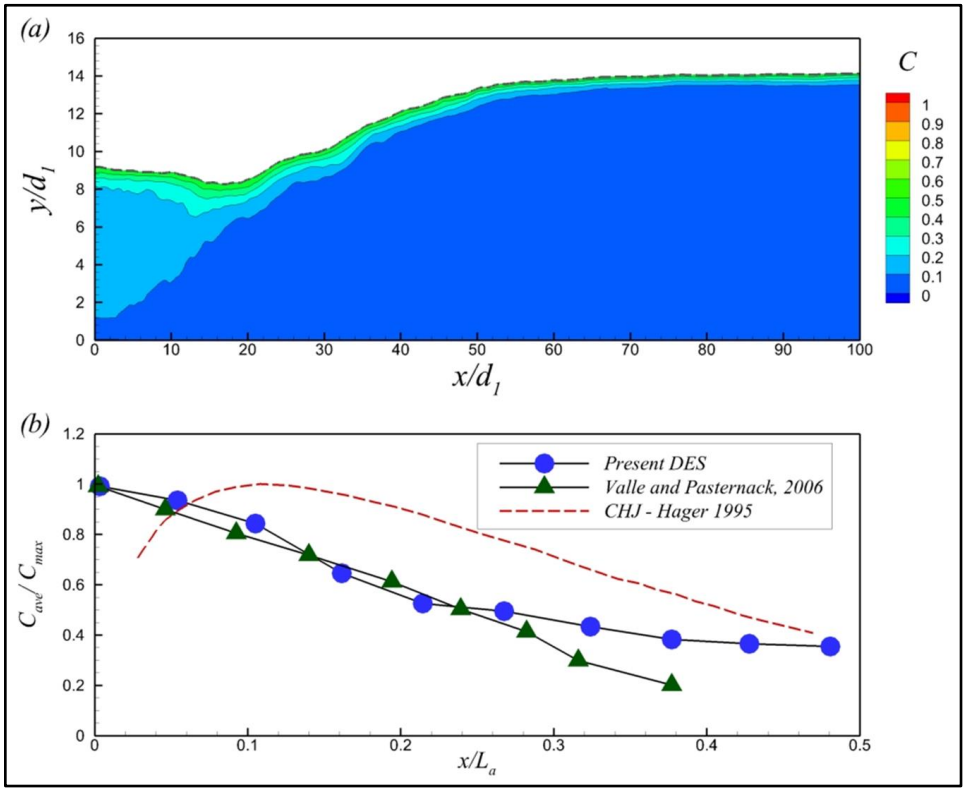

Figure 7: (a) Distribution of air concentration in the central plane of SHJ (b) Variation of average air concentration in the streamwise direction

In order to better understand the mechanism of air entrained in SHJ, numerical pressure probes, to collect time-dependent pressure data, were positioned at a height of d_1 at different streamwise locations along the channel. FFT analysis was carried out on the data collected for 10 s and the frequency of vortex shedding from the gate was found to be $f=13$ Hz. The time period $T= 1/f$ of the vortex shedding was split into eight time intervals. The contours of z-vorticity at the end of each time interval are presented in Fig. 8, to highlight the vortex shedding from the gate and to understand the interaction of these vortices with the free surface. At time $t = T/8$, it can be seen that a vortex has just been shed from the gate. The vortex shed from the gate is broken down into multiple smaller vortices 'A' and 'B' at $t = 2T/8$, due to the impact of the roller. The smaller vortex 'A' is pushed up towards the free surface by the accelerating influence of the roller, as observed at times $t = 3T/8$ and $t = 4T/8$. The flux of turbulent kinetic energy by the vortex is sufficient to cause the free-surface cusp to collapse and break the free-surface ($t = 5T/8$). This causes air entrainment into the SHJ. If the submergence factor of SHJ is large, the smaller vortices are completely broken down before they reach the surface and hence do not have enough intensity to cause the collapse and break-up of the free surface, leading to a reduction in the amount of air entrained. At $t =$

3T/8 it can also be seen that the smaller vortex 'B' is pushed towards the bed by the downwash caused by the roller and interact with the counter-rotating structures near the bed. This vortex is further broken down by the interaction with the bed and moves downstream without disturbing the free surface. Hence, it is evident Fig. 8 that the turbulent kinetic energy carried by the vortices are responsible for the breaking up of free surface and entraining air in the SHJ.

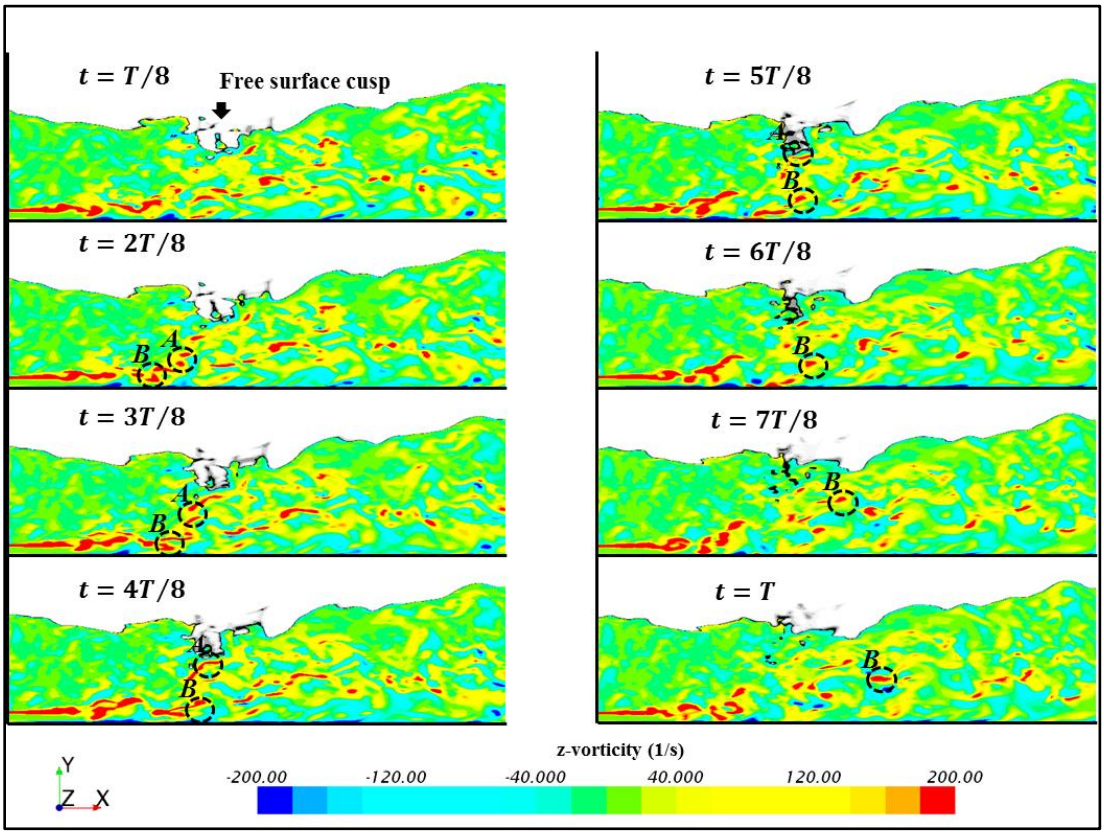

Figure 8: Mechanism of air entrainment in a submerged hydraulic jump

5 CONCLUSIONS

This study presents the results of a three-dimensional, unsteady, detached eddy simulation of a submerged hydraulic jump (SHJ) with an inlet Froude number 8.2 and a submergence factor of 0.24. The results showed that the numerical simulations were accurate in capturing the flow features of the SHJ. Since, the submergence factor of the present simulations is low, considerable amount of air is entrained into the flow. The simulations were accurate in predicting the air concentration in the flow. Large vortical structures shed from the sluice gate are broken down in the shear layer and the smaller vortices are pushed towards the free surface by the action of the roller. The turbulent kinetic energy carried by these vortices are sufficient to over come the surface tension, resulting in air entrainment.

REFERENCES

Chachereau, Y., and Chanson, H. 2011. Free-Surface Fluctuations and Turbulence in Hydraulic Jumps. *Experimental Thermal and Fluid Science* 35 (6): 896–909.

Chanson, H. 1995. Air Bubble Entrainment in Free-Surface Turbulent Flows: Experimental Investigations. https://espace.library.uq.edu.au/view.php?pid=UQ:9030.

Javan, M., and Eghbalzadeh, A. 2013. 2D Numerical Simulation of Submerged Hydraulic Jumps. *Applied Mathematical Modelling* 37 (10): 6661–6669.

Jesudhas, V. 2016. *Modeling of free-surface flows with air entrainment*. University of Windsor, Electronic Theses and Dissertations. Paper 5738

Jesudhas, V., Vesselina, R., Balachandar, R. and Barron, R. 2016. Submerged Hydraulic Jump Study Using DES. *Journal of Hydraulic Engineering*, 04016091.

Long, D., Steffler, P. M. and Rajaratnam, N. 1990. LDA Study of Flow Structure in Submerged Hydraulic Jump. *Journal of Hydraulic Research* 28 (4): 437–460.

Long, D., Steffler, P. M. and Rajaratnam, N. 1991. A Numerical Study of Submerged Hydraulic Jumps. *Journal of Hydraulic Research* 29 (3): 293–308.

Ma, F., Y. Hou, and P. Prinos. 2001. Numerical Calculation of Submerged Hydraulic Jumps. *Journal of Hydraulic Research* 39 (5): 493–503.

Rajaratnam, N. 1967. Hydraulic Jumps. *Advances in Hydroscience* 4 (1): 197–280.

Sarpkaya, T. 1996. Vorticity, Free Surface, and Surfactants. *Annual Review of Fluid Mechanics* 28 (1): 83–128.

STAR-CCM+, *User Guide v8.06*, 2013. CD-adapco.

Te Chow, Ven. 1959. *Open Channel Hydraulics*. McGraw-Hill Book Company, Inc; New York.

Vallé, Brett L., and Gregory B. Pasternack. 2006. Submerged and Unsubmerged Natural Hydraulic Jumps in a Bedrock Step-Pool Mountain Channel. *Geomorphology* 82 (1): 146–159.

Vischer, D. L., Willi H. Hager, and others. 1995. *Energy Dissipators*. Balkema Rotterdam.